REPORT DOCUMENTATION PAGE

Form Approved
OMB No. 0704-0188

Public reporting burden for this collection of information is estimated to average 1 hour per response, including the time for reviewing instructions, searching existing data sources, gathering and maintaining the data needed, and completing and reviewing this collection of information. Send comments regarding this burden estimate or any other aspect of this collection of information, including suggestions for reducing this burden to Department of Defense, Washington Headquarters Services, Directorate for Information Operations and Reports (0704-0188), 1215 Jefferson Davis Highway, Suite 1204, Arlington, VA 22202-4302. Respondents should be aware that notwithstanding any other provision of law, no person shall be subject to any penalty for failing to comply with a collection of information if it does not display a currently valid OMB control number. **PLEASE DO NOT RETURN YOUR FORM TO THE ABOVE ADDRESS.**

1. REPORT DATE *(DD-MM-YYYY)*	2. REPORT TYPE	3. DATES COVERED *(From - To)*
13-01-2009	Journal Article	

4. TITLE AND SUBTITLE

Experimental and Numerical Analysis of Radiometric Forces on a Heated Circular Vane in Argon (Preprint)

5a. CONTRACT NUMBER

5b. GRANT NUMBER

5c. PROGRAM ELEMENT NUMBER

6. AUTHOR(S)
N. Selden & C. Ngalande (USC); N. Gimelshein & S. Gimelshein (ERC); A. Ketsdever (AFRL/RZSA)

5d. PROJECT NUMBER

5f. WORK UNIT NUMBER
50260542

7. PERFORMING ORGANIZATION NAME(S) AND ADDRESS(ES)

Air Force Research Laboratory (AFMC)
AFRL/RZSA
10 E. Saturn Blvd.
Edwards AFB CA 93524-7680

8. PERFORMING ORGANIZATION REPORT NUMBER

AFRL-RZ-ED-JA-2009-012

9. SPONSORING / MONITORING AGENCY NAME(S) AND ADDRESS(ES)

Air Force Research Laboratory (AFMC)
AFRL/RZS
5 Pollux Drive
Edwards AFB CA 93524-7048

10. SPONSOR/MONITOR'S ACRONYM(S)

11. SPONSOR/MONITOR'S NUMBER(S)
AFRL-RZ-ED-JA-2009-012

12. DISTRIBUTION / AVAILABILITY STATEMENT

Approved for public release; distribution unlimited (PA #09033).

13. SUPPLEMENTARY NOTES
For publication in Physical Review E.

14. ABSTRACT

Radiometric force on a 0.12m circular vane is studied experimentally and numerically over a wide range of pressures that cover the flow regimes from near free molecular to near continuum. In the experiment, the vane is resistively heated to about 419 K on one side and 394 K on the other side, and immersed in a rarefied argon gas. The radiometric force is then measured on a nano-Newton thrust stand in a 3 m vacuum chamber and compared with the present numerical predictions and analytical predictions proposed by various authors. The computational modeling is conducted with a kinetic approach based on the solution of ES-BGK equation. Numerical modeling showed the importance of regions with elevated pressure observed near the edges of the vane for the radiometric force production. A simple analytic expression is proposed for the radiometric force as a function of pressure, that is found to be in good agreement with experimental data. The shear force on the lateral side of the vane was found to decrease the total radiometric force.

15. SUBJECT TERMS

16. SECURITY CLASSIFICATION OF:			17. LIMITATION OF ABSTRACT	18. NUMBER OF PAGES	19a. NAME OF RESPONSIBLE PERSON
					Dr. Andrew Ketsdever
a. REPORT	b. ABSTRACT	c. THIS PAGE	SAR	16	19b. TELEPHONE NUMBER *(include area code)*
Unclassified	**Unclassified**	**Unclassified**			N/A

Experimental and Numerical Analysis of Radiometric Forces on a Heated Circular Vane in Argon (Preprint)

N. Selden and C. Ngalande

University of Southern California, Los Angeles, CA 90089

N. Gimelshein and S. Gimelshein

ERC Incorporated, Edwards AFB, CA 93528

A. Ketsdever

University of Colorado at Colorado Springs, Colorado Springs, CO 80933

Abstract

Radiometric force on a 0.12 m circular vane is studied experimentally and numerically over a wide range of pressures that cover the flow regimes from near free molecular to near continuum. In the experiment, the vane is resistively heated to about 419 K on one side and 394 K on the other side, and immersed in a rarefied argon gas. The radiometric force is then measured on a nano-Newton thrust stand in a 3 m vacuum chamber and compared with the present numerical predictions and analytical predictions proposed by various authors. The computational modeling is conducted with a kinetic approach based on the solution of ES-BGK equation. Numerical modeling showed the importance of regions with elevated pressure observed near the edges of the vane for the radiometric force production. A simple analytic expression is proposed for the radiometric force as a function of pressure, that is found to be in good agreement with experimental data. The shear force on the lateral side of the vane was found to decrease the total radiometric force.

Distribution A: Approved for public release; distribution unlimited

INTRODUCTION

When a thin vane is immersed in rarefied gas, and a temperature gradient is imposed between the two sides of the vane either resistively or radiatively, a force will generally be exerted that will tend to move the vane from the hot to the cold side. Such a force is conventionally called radiometric, as it is identified with the forces acting in the Crookes radiometer [1, 2]. There has been little controversy regarding the cause of the radiometric forces at very low pressures since the explanation proposed by Tait and Dewar[3]. Here, the forces are due to molecules leaving the hotter surface with higher velocities than those leaving the colder one. This results in a pressure imbalance across the two surfaces, with the resultant net force in the direction from hot to cold. The sources of the radiometric forces at higher pressures are much less transparent, which has created a number of controversies in the past [2]. Even today, the issues does not seem to be fully settled [4]. It is important to note, however, that many of the explanations are based on a phenomenon called thermal transpiration [2], which was first explained by Reynolds.

The consequence of this explanation has been a number of radiometric force theories proposed over the years. One of the most rigorous explanations was proposed by Maxwell [5] and later improved by Hettner and Czerny [6]. This explanation contends that fluid particles will move from the cold side of the vane to the hot side. The reaction to this flow current is a force on the vane towards the cold side. The region where this force is observed is therefore the lateral sides of the vane. The tangential force of reaction on the vane per unit area is

$$\frac{3}{4}\frac{\eta^2}{\alpha\rho T}\frac{\partial T}{\partial x}, \tag{1}$$

where η is the coefficient of viscosity, ρ is the density, a is the distance to the opposite vane (or, generally, to the chamber walls), T is the temperature, and x is the length along the axis chosen parallel to the temperature gradient. Hettner and Czerny's force calculations compared favorably to earlier calculations by Knudsen who studied radiometric forces at higher pressures. The Hettner and Czerny's calculations were successful in explaining the radiometric forces in different settings. Using these calculations, it was possible to explain the Rubens and Nichols radiometers [7]. Their calculations were also extended to specify radiometric forces in other geometries including spheres. This analysis agreed with that of Sexl [8] who independently investigated a case of an ellipsoid of rotation and later a sphere.

These theories have also been successful in explaining photophoresis.

In 1924, A. Einstein published a paper putting forward a theory of radiometric force [9]. His theory, as with the Hettner and Czerny calculations, is based on some elements of the thermal transpiration phenomenon. According to the Einstein's derivation, the force acting on the vane perimeter,

$$p\lambda\frac{\Delta T}{T}, \tag{2}$$

where p is gas pressure, λ is the gas mean free path, ΔT is the temperature difference, and T is the absolute temperature. The force in Eqn. (2) is produced in an area that is one mean free path thick, and is given per unit length of the edge. This theory found partial confirmation in the experiments by Marsh [10]. Later, Sexl showed that Einstein's theory was deduced from a reasoning which was not strictly accurate; he modified the theory and derived an expression for the radiometric force on a dish radiometer [8] as

$$\frac{14.72}{n+5}\frac{p\lambda^2}{T}\Delta T, \tag{3}$$

where n is the number of active internal degrees of freedom of gas molecules (0 for a monatomic gas). The main difference between Sexl and Einstein's formulas is that Sexl's radiometric force is inversely proportional to gas pressure while Einstein's force is independent of pressure and is proportional to the perimeter of the vane. Even though there is a pressure term in Eqn (2), this term cancels out with the mean free path term and becomes a constant independent of pressure [2]. It must also be emphasized that Eqn (2) assumes the radiometric force to act only within a single mean free path from the edge.

A general expression that is consistent with the bell-shaped dependence of the radiometric force on pressure, consistent with many experimental studies was proposed by Westphal [11], $F \propto \frac{p}{a} + \frac{1}{bp}$, where a and b are geometry and gas dependent constants. Note that the interest in radiometric phenomena significantly reduced after 1930s, but started to grow rapidly in the last decade, primarily because radiometric phenomena were found to be useful in a number of different micro- and large scale devices. One of the most important of these is atomic force microscopy (AFM), a research field that, although invented back in 1986 [12], has been brought to the forefront of modern nanotechnologies in the last several years (see, for example, [13–15]). The use of radiometric forces as an approach to study gas-surface translational energy accommodation has been suggested by Passian et al. in Ref. [16]. A

new concept of a high-altitude aircraft supported by microwave energy that uses radiometric effects has also been put forward in Ref. [17].

Most recently, Scandurra et al have derived a new expression for radiometric force, that has both pressure and shear components [4]. For the normal force per unit area on a thin vane, they obtained

$$(2 - \alpha_E)\frac{15k}{32\sqrt{2}\pi\sigma^2}\Delta T l, \tag{4}$$

where α_E is the energy accommodation coefficient, k is the Boltzmann constant, $\pi\sigma^2$ is the total collision cross section, and l is the vane perimeter. For the shear force per unit area, the expression is

$$\alpha_E\frac{15k}{64\sqrt{2}\pi\sigma^2}\frac{\Delta T}{\lambda}(\tau l), \tag{5}$$

where τ is the vane thickness. One of the important assumptions of this work is constant pressure in the gas surrounding the heated vane.

The main objectives of this work are the experimental and numerical study of the accuracy of different estimates of the radiometric forces, the quantitative analysis of the pressure gradients near the radiometer vane, and the evaluation of the associated edge effects and their relative importance in the radiometric forces. Direct experimental measurements of a force on a resistively heated aluminum vane immersed in argon gas are conducted in the pressure range where the force is near its maximum. The measurements are complemented by numerical modeling that is based on a kinetic approach, namely a solution of the ES-BGK model kinetic equation, which allows detailed analyzes of gas flow near the vane and surface force distributions. Qualitative analysis of the edge force mechanisms allowed the authors to propose a simple analytic expression for a quick estimate of the radiometric forces.

EXPERIMENTAL SETUP AND NUMERICAL APPROACH

To study the effects of the argon gas pressure on the production of radiometric forces on a vane, a circular plate device was used. The device consisted of a Teflon insulator placed between two aluminum plates, with each plate having a thickness of 0.318 cm. A resistive heater was affixed between one of the aluminum plates and the Teflon insulator, and the entire device was assembled using eight low-conductivity nylon machine screws with 2.13 mm diameters. The assembled device has a total thickness of 0.95 cm, with a diameter of 11.13 cm and is shown in Fig. 1. When coupled with a DC power supply the

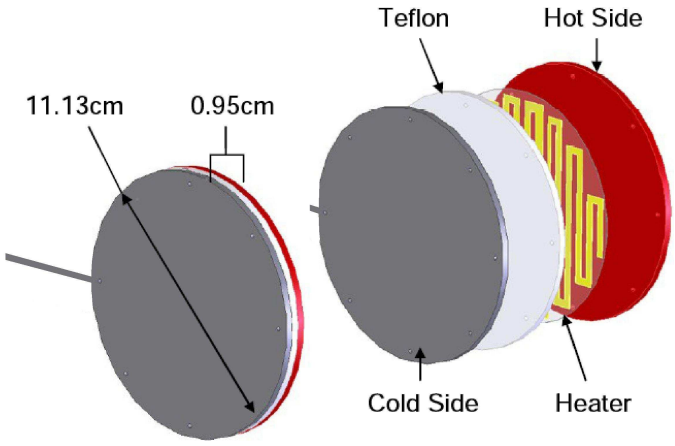

FIG. 1: CAD drawing of the radiometric device.

resistive heater was used to maintain a consistent power input of approximately 8 W to the radiometer vane, and the entire device was allowed to come to thermal equilibrium under vacuum.

The radiometer was mounted on a modified version of the nano-Newton Thrust Stand (nNTS) [18] located inside the 3.0 m diameter vacuum chamber. When calibrated using a set of electrostatic combs [19], the nNTS provides very accurate and repeatable data with typical force resolution of approximately 0.1μN and statistical scatter around 1%. For the current setup, the experimental error based on standard deviation ranges from a few percent at the lowest pressures to less than 1% through most of the curve. However, due to the normalization by experimental temperature measurements, variation of the background pressure, and the small uncertainty of the calibration method, the total absolute experimental uncertainty is about 4%. Day-to-day variation of multiple data sets has been observed to be approximately 2%.

The experimental data was obtained by evacuating the chamber to a base pressure below 10^{-3} Pa. A constant voltage was applied to the heater, and this resulted in the main surfaces reaching temperatures of approximately 419 K (hot) and 394 K (cold). The background pressure inside the chamber was varied by filling the chamber with argon, helium, and nitrogen over a range of pressures from 0.1 Pa to 1.0 Pa. The experimentally measured force was normalized by the temperature difference between the hot and cold plates, ΔT, for the purpose of comparing results for different pressures and chambers. Verification of the validity of the experimental normalization method is demonstrated in a previous paper

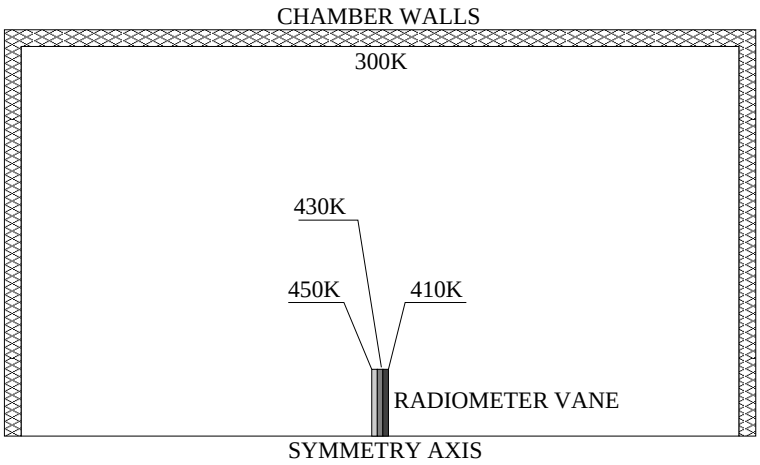

FIG. 2: Computational setup.

[20], where exceptional linearity with temperature difference is observed.

A finite volume solver SMOKE developed at ERC has been used to deterministically solve the ES model kinetic equation. SMOKE is a parallel code based on conservative numerical schemes developed by L. Mieussens [21]. The code has both two-dimensional and axisymmetric capabilities. A second order spatial discretization is used along with implicit time integration. Fully diffuse reflection with complete energy accommodation is applied at the vane and chamber walls. A symmetry plane (symmetry axis in axisymmetric computations) was set at the lower boundary. Two computational domains have been used, 0.44 m$\times$0.22 m and 3 m$\times$1.5 m. For the smaller, domain, a smaller, 0.039 m diameter, vane was used. The use of the smaller domain allowed modeling of radiometric flows at very low Knudsen numbers (below 0.01), while the use of the larger domain allowed for direct comparison with the experimental data. The grid convergence was achieved by increasing the number of spatial nodes and points in the velocity space. The latter one was (18,18,12) for the results presented below, and the number of spatial cells varied from 5,000 to 50,000 depending on the chamber size. The temperature and geometric setup is illustrated in Fig. 2. Note that the temperature of the lateral side of the vane is set as a piecewise constant with three different temperature values (cold side temperature, hot side temperature, and the average between them).

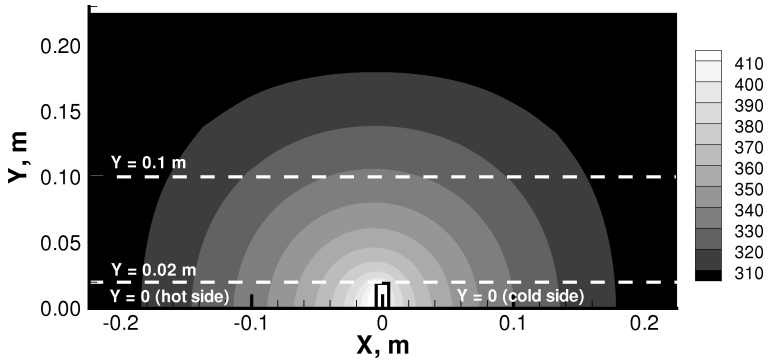

FIG. 3: Temperature field around the radiometer vane, 2 Pa.

RESULTS AND DISCUSSION

Consider first the numerical solution obtained in a small chamber for an argon pressure of 2 Pa. The temperature field for this case is presented in Fig. 3. For this intermediate Knudsen number, about 0.07 based on the vane diameter, there is a noticeable temperature jump at the heated radiometer vane surfaces, which exceeds 10 K at the center of the vane. The temperature then quickly decreases to its free stream value of 300 K, with the rate of decrease being approximately the same in all directions. The quantitative behavior of the gas temperature is shown in Fig. 4 where the temperature profiles are presented along the dashed lines plotted in Fig. 3. The temperature gradient is highest at the center of the vane (y = 0) on both hot and hot cold sides, which differs somewhat from the assumption made in the theoretical model developed in Ref. [4]. There, the gradients along the lateral side of the vane were assumed to be stronger than those near the center due to a thin vane geometry.

Another important assumption made in [4] is that of a constant pressure near the radiometer vane. A close-up view of the pressure field in the vicinity of the radiometer is given in Fig. 5. The lower half of the flow is a mirror of the upper half; it is shown to provide a better picture of the flow. The conclusion here is that not only the pressure is different at the cold and hot sides of the vane, as well as along the lateral sides, but also that the pressure changes along both the hot and the cold sides. There are regions of high pressure being formed near the edges of the vane. Even though the gas pressure in these regions is only about 0.5% larger than the corresponding values near the center, this difference is close

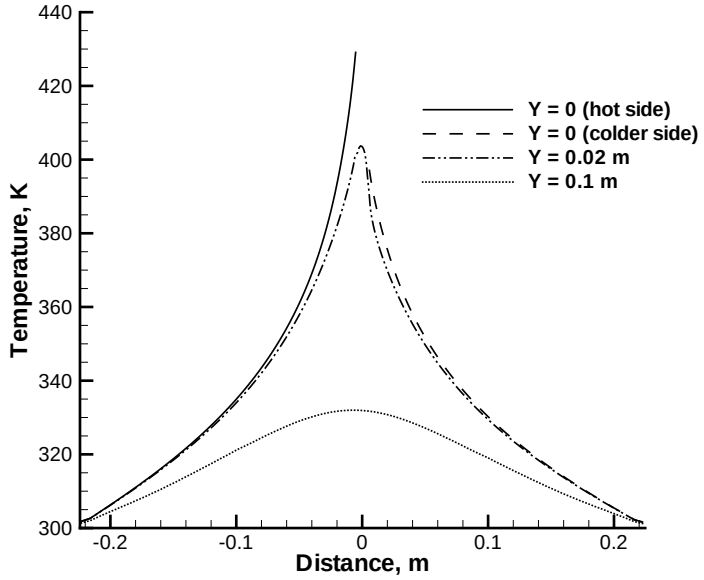

FIG. 4: Temperature profiles along different cross sections parallel to the symmetry axis.

to the difference between the pressure near the hot and cold sides for a given value of Y. Therefore it is critical for the radiometric force production.

Figure 6 shows the computed distribution of the surface pressure difference between the hot and the cold sides for different gas pressures in 2D case (i.e. in effect the pressure component of the radiometric force). The pressure difference, that is uniform for a free molecular flow, is still nearly constant along the vane for a pressure of 0.305 Pa (Knudsen number about 0.4). For a pressure of 1.219 Pa, for which the radiometric force is close to maximum, there is a visible difference between the force production near the center and near the edge, with the latter being about two times larger. The difference sharply increases with pressure, and at 18 Pa there is no force production in the central part of the vane (the pressure is equilibrated between the hot and the cold sides). Most of the force is created within about ten mean free paths from the outer edges of the vane.

The computations clearly show that, for a collisional flow, the force on the working side of the vane reaches its maximum near the edge. The formation and the existence of this maximum may be qualitatively explained as follows. Analyzing the molecular fluxes on the two small regions, each with the size equal to the gas mean free path near the vane edge, λ,

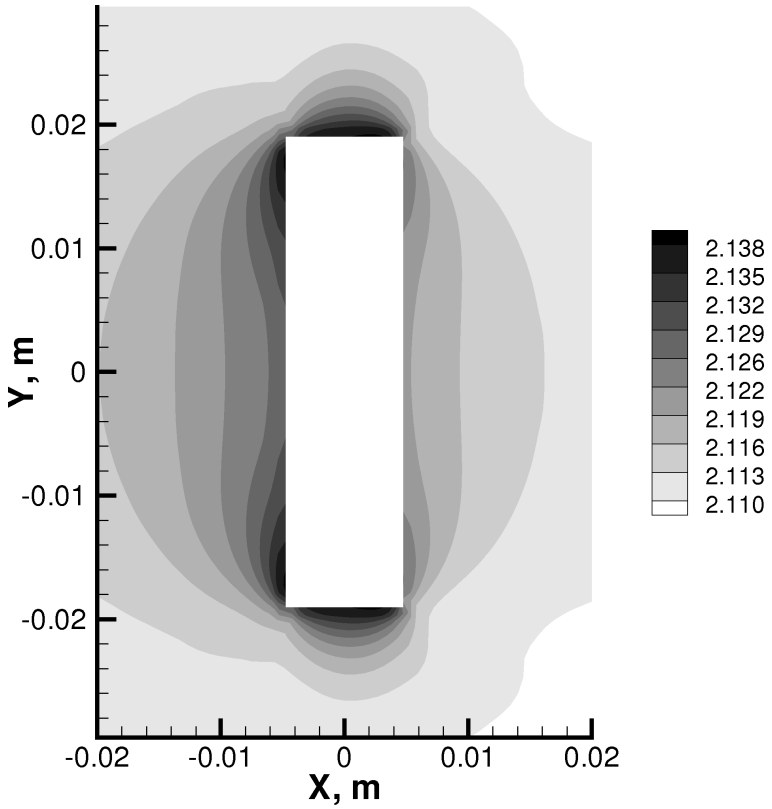

FIG. 5: Pressure distribution around the vane.

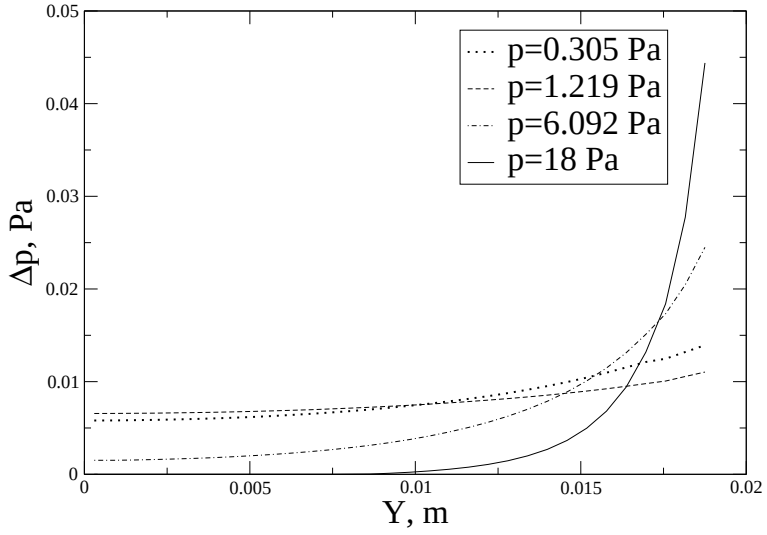

FIG. 6: Surface pressure difference between the hot and the cold sides of the vane for various gas pressures.

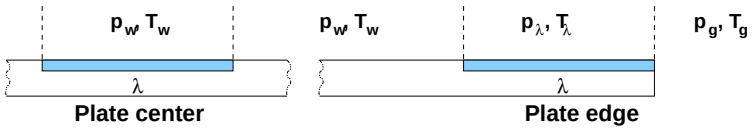

FIG. 7: Schematics of the gas conditions near the radiometer vane.

the mean free path is assumed to be significantly smaller than the vane size. One of these regions is located near the center of the vane, and the other is adjacent to the vane edge, as schematically shown in Fig. 7. Consider first the region located near the center of the vane. The flux on this region is determined by the gas conditions above it (between the dashed lines) as well as the gas conditions to the left and to the right of this region, as molecules coming on the surface may cross the dashed lines. Since the gas mean free path is small compared to the vane size, the gas conditions (both pressure and temperature) above the central region and to the sides of it are approximately the same, and may be denoted as p_w and T_w, respectively.

The bulk flow velocity near the vane is very small in radiometric flows, and its contribution to the total pressure on the working side of the vane is negligible. The inward number flux on the central region may generally be written as

$$\dot{N} = n_w \int_{-\infty}^{\infty} \int_{-\infty}^{\infty} \int_{0}^{\infty} muf_w \mathrm{d}c_x \mathrm{d}c_y \mathrm{d}c_z. \tag{6}$$

Here, c_x is the velocity in the direction normal to the vane, c_y and c_z are the tangential velocities, n_w is the number density near the central region, and f_w is the velocity distribution function. When the gas is close to equilibrium, the number flux on a stationary vane may be approximated as $\dot{N} \approx n\bar{c}/4$.

The principal difference between the central and edge regions in terms of the inward number flux is that for the latter this flux is determined not only by gas state immediately above the vane but also by gas to the right of the vane. In this area, the gas has pressure p_g and temperature T_g. Whereas the pressure is expected to be close to the pressure near the surface, $p_g \approx p_w$, the temperature there is obviously lower, $T_g < T_w$. Let us denote the temperature ratio R, $R = \frac{T_g}{T_w} < 1$. Since the pressure values are approximately the same, the number density ratio will then be $\frac{n_g}{n_w} = R^{-1} > 1$. Then the ratio of the number fluxes based on molecules coming to the central and edge regions from the right may be approximated as $\frac{\dot{N}_g^{right}}{\dot{N}_w^{right}} \approx R^{-\frac{1}{2}} > 1$. Therefore, while initially the momentum fluxes on the central and edge

regions may be similar, the number flux on the edge region is larger. Since molecules are assumed to undergo complete momentum and energy accommodation on the surface, such an inequality in number fluxes results in a slight increase in pressure near the edge of the vane. Due to molecular collisions, this increase eventually causes a higher momentum flux on the edge.

Note that since the relaxation scale amounts to several mean free paths, the actual size of the edge region with elevated pressure is larger than a single mean free path. This qualitative analysis is expected to be applicable to some extent even for cases when mean free path is comparable to the size of the vane. When the gas mean free path is much larger than the radiometer size, the free molecular expression may be used for the radiometric force, is given by

$$\frac{p}{2}A\left(\sqrt{\frac{\alpha_E T_h + (1-\alpha_E)T_g}{T_g}} - \sqrt{\frac{\alpha_E T_c + (1-\alpha_E)T_g}{T_g}}\right), \tag{7}$$

where T_h and T_c are the hot and the cold temperatures, respectively, and T_g is the free stream gas temperature. Generally, the energy accommodation coefficients may be different on different sides of the vane. Here, A is the area of the radiometer. Keeping in mind that with the increase of gas pressure the surface area where the radiometric force is significant will decrease, an effective area may be introduced for a circular vane as

$$A = \pi R_{eff}^2 = \pi R^2 - \pi(R - n\lambda)^2, \tag{8}$$

where R is the vane radius, λ is the mean free path of the ambient gas, and $n\lambda$ specifies the thickness of the edge area where the force is produced. Note that in the limit of $\lambda \to 0$ the force produced becomes independent of pressure, similar to Eqn. (2).

If an assumption similar to Einstein's is made, and $n = 1$ is used, the radiometric force computed with a simple analytic expression (Eqn. (7)) gives surprisingly close agreement with the present experimental results, as shown in Fig. 8. It is interesting to note that the assumption of $n = 1$ works very well, even though it has been shown above that the pressure imbalance occurs over a region of ten mean free paths. When the energy accommodation coefficient of one is used, the values calculated using the analytical model somewhat overpredict the experimental data. When an accommodation coefficient of 0.8 is used, close to some of experimental recommendations [22], the estimated maximum force is only a few percent higher than the experimental value. Note that Eqn (8) applied for a circular radiometer may be easily modified for any other geometric shape.

Distribution A: Approved for public release; distribution unlimited

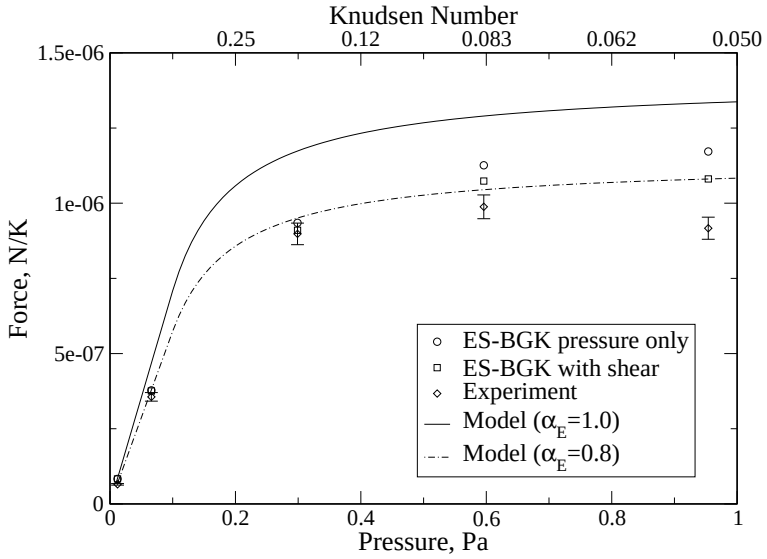

FIG. 8: Experimental and calculated force on the vane for different pressures.

Figure 8 also presents the results of the numerical solution of the ES-BGK equation (the large domain case is presented here). Two sets of data points are given: (i) the full radiometric force that include both pressure force on the working side of the vane and the shear force on the lateral side of the vane, (ii) the radiometric force without the shear. The full radiometric force is somewhat larger than the experimental data due to several reasons. First, and most important, the actual surface accommodation both on the vane and on the chamber walls is not fully diffuse. An accommodation coefficient lower than unity will obviously decrease the computed force value. Second, the ES-BGK equation is an approximation to the Boltzmann equation, the most general equation that describe dilute gas flows, and its solutions may deviate somewhat from the solution of the full Boltzmann equation. Third, there is are uncertainties inherent both in the experimental (estimated to be up to 4%) and numerical (up to 3%, based on the convergence patterns and the estimation of the numerical parameter effects) modeling results.

Comparison of the ES-BGK results shows that the combined shear force is acting toward the reduction of the total radiometric force, contrary to what was previously assumed by several authors [4, 6]. The shear force is practically nonexistent at the lowest pressures under consideration, but increases to almost 8% for the pressures where the force is near its maximum. Note that the authors have validated this fact with additional simulations using the direct simulation Monte Carlo (DSMC) method, a statistical approach to the solution

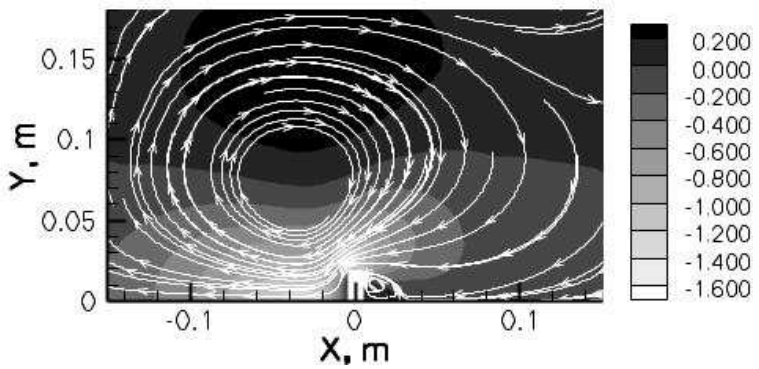

FIG. 9: Velocity streamlines around the radiometric vane, 2 Pa.

of the Boltzmann equation. The DSMC computations also resulted in a shear force acting opposite to the pressure force. The negative shear force may be explained when considering the ES-BGK distribution of flow velocities and streamlines, shown in Fig. 9 in the vicinity of the vane for a chamber pressure of 2 Pa and the small domain case. The temperature gradients generate two counter-propagating vortices in the upper half of the flow, a very large vortex centered above the vane closer to the hot side, and a much smaller vortex adjacent to the cold side. Among the sources that create these vortices may be the local pressure maxima near the edges of the vane, that move gas toward the center both at the cold and hot sides. The larger vortex creates a combined force on the lateral side of the vane that is directed from cold to hot side.

Finally, Fig. 10 presents the comparison of the radiometric force estimates obtained using analytical expressions proposed by different authors, with the present experimental data. Although the expression in Ref. [8] does not capture the correct trend for smaller pressures, it still produces a reasonable estimate for pressures that correspond to the maximum force in the experiment. The expression in Ref. [4] significantly overpredicts the experimental data, and the expression of Ref. [9] underpredicts the maximum force.

CONCLUSIONS

An experimental and computational study of the radiometric force has been performed for an argon gas in a wide range of pressures. Accurate measurements of the radiometric force on a resistively heated 0.12 m diameter circular vane were conducted with a nano-Newton

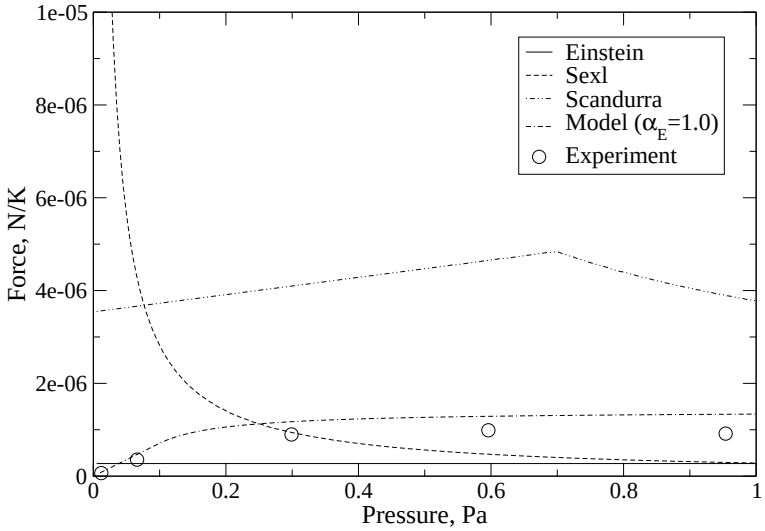

FIG. 10: Force prediction according to different models.

thrust stand in a 3 m vacuum chamber for pressures between 0.01 and 1 Pa. A kinetic approach based on the solution of the ES-BGK equation has been applied to numerically analyze the radiometric flow for pressures from 0.01 to 18 Pa.

The numerical results demonstrated the existence of regions with elevated gas pressure. A qualitative explanation of the formation of these regions is given and a simple expression that allows a quick estimate of the radiometric force as a function of pressure is suggested. The force predictions obtained with this expression are in a good agreement with the experimental data. The ES-BGK results somewhat overpredict the experimental data, which is primarily attributed to the fully diffuse energy accommodation used in the calculations.

The force production was found to be nearly constant along the vane for pressures smaller than those where the force is maximum, and strongly shifted toward the edge for higher pressures. Generally the region of the force production was about ten mean free paths thick. The shear force exerted on the lateral side of the radiometer vane was found to decrease the total radiometric force. Finally, various expressions for the radiometric force, suggested in literature, were evaluated through the comparison with the experimental data. A simple model that gives reasonable agreement with experimental data was proposed.

The work at USC and ERC was supported in part by the Propulsion Directorate of the Air Force Research Laboratory at Edwards Air Force Base, California. The work at ERC was supported by AFOSR. The authors thank Dr. Ingrid Wysong and Dr. E.P. Muntz for

many fruitful discussions.

---

[1] W. Crookes, Phil. Trans. R. Soc., **163** 277 (1873).

[2] L.B. Loeb, *The kinetic theory of gases*, Dover Publications Inc., (1961).

[3] P.G. Tait and J. Dewar, Nature **12** 217 (1875).

[4] M. Scandurra, F. Iacopetti, P. Colona, Physical Review E **75** 026308 (2007)

[5] J.C. Maxwell, Phil. Trans. R. Soc., **170** 231 (1879).

[6] G. Hettner and M. Czerny, Z. Physik **30** 258 (1924).

[7] H. Rubens and E.F. Nichols, Wied. Ann **60** 401 (1897).

[8] Th. Sexl, Z. Physik, **52** 249 (1929).

[9] A. Einstein, Z. Physik, **27** 1 (1924)

[10] H. E. Marsh, J. Opt. Soc. Amer., **12**, 135 (1926)

[11] W. H. Westphal, Zeit. fur Physik, **1**, 92 (1920)

[12] G. Binning, C. F. Quate, Ch. Gerber, Phys. Rev. Lett., **56**, 930 - 933 (1986)

[13] F. Giessibl, Advances in Atomic Force Microscopy, Reviews of Modern Physics, **75** (3), 949-983 (2003).

[14] P. Hinterdorfer, Y. F. Dufrne, Nature Methods **3**, 347 - 355 (2006).

[15] B. Gotsman, U. Durig, Appl. Phys. Letters, **87** 194102 (2005).

[16] A. Passian, R. J. Warmack, T.L. Ferrell, T. Thundat, Phys. Rev. Letters, **90**(12) 124503 (2003).

[17] G. Benford, J. Benford, Acta Austonautica, **56**, 529 (2005).

[18] A.J. Jamison, A.D. Ketsdever, E.P. Muntz, Review of Scientific Instruments **73** 3629 (2002).

[19] N.P. Selden, A.D. Ketsdever, Review of Scientific Instruments **74** 5249 (2003).

[20] N. Selden, C. Ngalande, S. Gimelshein, and A. Ketsdever, AIAA Paper 2007-4403 (2007).

[21] L. Mieussens, Journal of Computational Physics **162** 429 (2000).

[22] S.C. Saxena, R.K. Joshi, *Thermal accommodation and adsorption coefficients of gases*, Hemisphere Publishing Corp, New York (1989)